ЖЭТФ, 2001, том 120, вып. 3 (9), стр. 700–711

SUPERCONDUCTIVITY IN $Ba_{1-x}K_xBiO_3$: POSSIBLE SCENARIO OF SPATIALLY SEPARATED FERMI–BOSE MIXTURE

A. P. Menushenkov, K. V. Klementev, A. V. Kuznetsov

Moscow State Engineering Physics Institute
115409, Moscow, Russia

M. Yu. Kagan

P. L. Kapitza Institute for Physical Problems
117334, Moscow, Russia

Submitted 16 March 2001

We propose a new scenario for the metal–insulator phase transition and superconductivity in the perovskite-like bismuthates $Ba_{1-x}K_xBiO_3$ (BKBO) based on our EXAFS studies. We show that two types of charge carriers, the local pairs (real-space bosons) and the itinerant electrons, exist in the metallic compound $Ba_{1-x}K_xBiO_3$ ($x \geq 0.37$). The real-space bosons are responsible for the charge transport in semiconducting $BaBiO_3$ and for superconductivity in the metallic BKBO. The appearance of the Fermi-liquid state as the percolation threshold is overcome ($x \geq 0.37$) explains the observed metal–insulator phase transition. Because bosons and fermions occupy different types of the octahedral BiO_6 complexes, they are separated in real space, and therefore, the spatially separated Fermi–Bose mixture of a new type is likely to be realized in the bismuthates. The nature of superconductivity is consistently explained in the framework of this scenario. A new superconducting oxide $Ba_{1-x}La_xPbO_3$ has been successfully synthesized to check our conclusions.

PACS: 74.20.Mn, 74.72.Yg

1. INTRODUCTION

The concept of the extremely strong-coupling superconductivity with preexisted local pairs was first introduced by Shafroth [1] in the middle of the fifties. His statement was that in the extremely type-II superconductors, where $\xi_0 k_F \lesssim 1$, the nature of the superconducting transition corresponds to the local pair formation (pairing in the real, rather than in the momentum space) at some relatively high temperature T^* and to the Bose–Einstein condensation (BEC) of pairs at a lower critical temperature $T_c < T^*$. Later on, Alexandrov and Ranninger developed this concept [2] for narrow-band materials with an extremely strong electron–phonon coupling constant ($\lambda \gg 1$), where the standard Eliashberg theory [3] becomes inadequate. The key issue of their approach was the statement that in narrow bands, where the polaron formation is important, it is possible, in principle, to create the conditions for two polarons to effectively occupy the same potential well prepared within a self-consistent procedure.

At approximately the same time, Leggett and Nozieres [4, 5] developed a general theory that described a smooth interpolation between the BCS-type pairing in the momentum space for a weak electron–electron attraction and the pairing in the real space for a strong electron–electron attraction. There were two crucial points in their papers [4, 5]. (i) The results are valid independently of the actual nature of the short-range effective attraction between electrons; (ii) they have self-consistently investigated the standard equation for the superconducting gap and the equation for the conservation of the number of particles. The most important result of Nozieres and Leggett is that for $T^* > T_c$ (in other words, for the binding energy of a local pair $|E_b| > \varepsilon_F$), one has a normal bosonic metal that is responsible for the electron transport. Later on, Ranninger [6, 7] introduced the concept of the two-band Fermi–Bose mixture. His scenario involves the contributions of fermionic and bosonic quasiparticles to the electron transport for $T_c < T < T^*$.

Soon after the discovery of high-T_c superconduc-

tors, Anderson [8] reintroduced the concept of local pairs. He also used two bands of the fermionic and bosonic quasiparticles. In his approach, the superconducting transition was related to the BEC in the bosonic band of charge excitations, the holons, while the presence of a large Fermi surface was guaranteed by the fermionic band of spin excitations, the spinons. Unfortunately, even this beautiful approach was not totally successful because at least in one layer, the BEC of holons yields the superconductive pair charge e instead of $2e$ measured experimentally.

Later on, Geshkenbein, Ioffe, and Larkin [9] phenomenologically reconsidered the model of the Fermi–Bose mixture at the level of the Ginzburg–Landau expansion coefficients and showed that several important experiments in the underdoped high-T_c materials can be naturally explained within this form of the Ginzburg–Landau functional. At present, therefore, the question of whether a two-band Fermi–Bose mixture scenario is applicable to high-temperature superconducting (HTSC) materials remains open. The materials that can be best described by this scenario are the bismuth family of high-T_c superconductors $Bi_2Sr_2CaCu_2O_{8+\delta}$, where $k_F\xi_0 \approx 2$, and the tunneling experiments of Rener et al. [10] signal the formation of a sufficiently large and stable pseudogap at temperatures well above T_c.

In this paper, we discuss the possibility of a two-band Fermi–Bose mixture scenario in an entirely different class of superconductors with a relatively high critical temperature $T_c \sim 30\,\mathrm{K}$, namely in the barium bismuthates $Ba_{1-x}K_xBiO_3$. The key issue of our paper is the possibility of the existence of spatially separated subsystems of fermionic and bosonic quasiparticles in these materials. The cubic perovskites $BaPb_{1-x}Bi_xO_3$ (BPBO) and $Ba_{1-x}K_xBiO_3$ (BKBO) have been known and extensively studied since 1975 and 1988 respectively. A large number of the first-principle calculations have been carried out [11–17] to explain the high-temperature superconductivity in these compounds. However, most of the unusual properties of the $BaBiO_3$-family compounds mentioned in the early review by Uchida et al. [18] still remain unexplained. From our point of view, the reason is that these calculations were done in the mean-field approximation, and therefore, they adequately describe crystal structures with the translational symmetry but cannot explain the peculiarities of the electronic properties of BPBO and BKBO following from the local structure distortions. Such distortions, which were observed by the local sensitive methods such as the XPS [19], Raman scattering [20], and EXAFS [21–24], destroy the translation symmetry. Therefore, the mean-field approximation cannot describe the local electronic structure.

Based on the low-temperature EXAFS study of the BKBO and BPBO compounds, the motion of the local electronic pairs correlated with the lattice vibrations was established in our recent work [22]. We found that different electron fillings of the upper antibonding $Bi6s$–$O2p_{\sigma^*}$ orbital of the BiO_6 octahedra lead to the formation of a double-well potential for the vibration of some part of the oxygen ions. The observed anomalies have been discussed in the framework of different theoretical models of superconductivity. We found that none of them can fully explain our experimental results and proposed a phenomenological model of the relationship between the local crystal and the local electronic structures.

We here present a relatively new concept of superconductivity in bismuthates based on an interplay between spatially separated Fermi and Bose subsystems. In contrast to the previous theoretical models and calculations, we take the results obtained in a number of local sensitive measurements into account [19–24].

The paper is organized as follows. In Sec. 2, we present the basic experimental facts pertaining to the local electronic and crystal structure peculiarities and consider their relation to the superconducting and the normal transport properties of BKBO. We then show how these basic facts can be naturally explained within the scenario of two spatially separated bands of the fermionic and bosonic quasiparticles. In Sec. 3, consequently, we discuss the nature of superconductivity in the bismuthates within this scenario. We conclude the paper by summarizing our model and discussing several additional experiments that would help give a definite answer as to whether our proposal is the only possibility for a superconducting pairing in bismuthates.

2. SPATIALLY SEPARATED FERMI–BOSE MIXTURE

$BaBiO_3$, which is a parent compound for the bismuthates $Ba_{1-x}K_xBiO_3$ and $BaPb_{1-x}Bi_xO_3$, represents a charge-density-wave (CDW) insulator having two gaps: an optical gap with $E_g = 1.9\,\mathrm{eV}$ and an activation (transport) gap with $E_a = 0.24\,\mathrm{eV}$ [18]. A partial replacement of Ba by K in BKBO causes the decrease of the gaps, and as a result, the insulator–metal transition and superconductivity are observed at the doping levels $x \gtrsim 0.37$. The superconductivity remains up to the doping level $x \approx 0.5$ corresponding to the so-

lubility limit of K in BKBO, but the maximum critical temperature $T_c \approx 30$ K is achieved for $x \approx 0.4$ [25, 26].

A. Local crystal structure peculiarities

A three-dimensional nature of the cubic perovskite-like structure of the bismuthates differs from the two-dimensional one in the HTSC cuprates. The building block in the bismuthates is the BiO_6 octahedral complex (the analogue of CuO_n ($n = 4, 5, 6$) in HTSC materials). The octahedral complexes are the most tightly bound items of the structure because of a strong covalence of the Bi6s–O2p_σ bonds. According to the crystallographic data [27], the crystal structure of a parent $BaBiO_3$ compound represents the alternating arrangement of the expanded and contracted BiO_6 octahedra (referred to as the «breathing» distortion) in the barium lattice. This alternation and the static rotation of the octahedra around the axis [110] produce a monoclinic distortion of the cubic lattice. As shown in Refs. [21, 22, 28], the larger soft octahedron corresponds to the BiO_6 complex with the completely filled Bi6s–O2p orbitals and the smaller rigid octahedron corresponds to the $Bi\underline{L}^2O_6$ complex. Here, $\underline{L}^2$ denotes the free level in the antibonding Bi6s–O2p_{σ^*} orbital of the smaller octahedral complex.

The K doping of $BaBiO_3$ is equivalent to the hole doping and leads to a partial replacement of the larger soft octahedra BiO_6 by the smaller rigid octahedra $Bi\underline{L}^2O_6$ [22]. This causes the decrease and the eventual disappearance of the static breathing and tilting distortions; the lattice must therefore contract despite the practically equal ionic radii of K^+ and Ba^{2+}. As a result, the average structure becomes a simple cubic one at the doping level $x = 0.37$ in accordance with the neutron diffraction data [29]. However, the local EXAFS probes [21, 22, 24] showed a significant difference of the local crystal structure from the average one. We found that the oxygen ions belonging to the different BiO_6 and $Bi\underline{L}^2O_6$ octahedra vibrate in a double-well potential, while those having an equivalent environment of the two equal $Bi\underline{L}^2O_6$ octahedra oscillate in a simple harmonic potential [21, 22]. This very unusual behavior is closely related to the local electronic structure of BKBO.

B. Local electronic structure

The coexistence of the two types of the octahedra in $BaBiO_3$ with different Bi–O bond lengths and strengths reflects the different electronic structures of BiO_6 complexes. The valence band of $BaBiO_3$ is determined

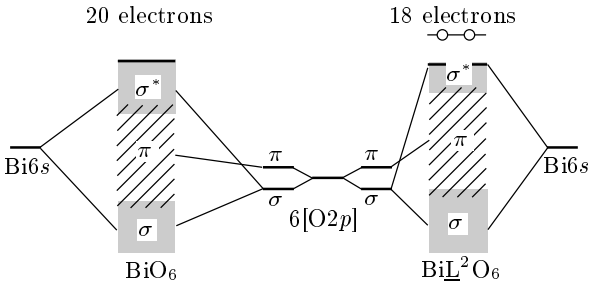

Fig. 1. The scheme of the formation of an electronic structure for the different octahedral BiO_6 complexes

by the overlap of the Bi6s and O2p orbitals [11, 30], and because of a strong Bi6s–O2p_σ hybridization, the octahedra can be considered as quasimolecular complexes [31]. Each complex involves ten electron levels consisting of four bonding–antibonding Bi6s–O2p_σ orbitals and six nonbonding O2p_π orbitals. A monoclinic unit cell includes two octahedra and contains 38 valence electrons (10 from two bismuth ions, 4 from two barium ions, and 24 from six oxygen ions). All the Bi–O bond lengths must be equal and local magnetic moments must be present for the equal electron filling of the nearest octahedra ($Bi\underline{L}^1O_6 + Bi\underline{L}^1O_6$). However, the presence of two types of octahedral complexes and the absence of any local magnetic moment were observed experimentally [18, 32]. A scheme of the valence disproportionation $2Bi\underline{L}^1O_6 \rightarrow Bi\underline{L}^2O_6 + BiO_6$ was then proposed [22] in which the numbers of occupied states are different in the neighboring octahedral complexes: the octahedron $Bi\underline{L}^2O_6$ contains 18 electrons and has one free level or a hole pair $\underline{L}^2$ in the upper antibonding Bi6s–O2p_{σ^*} orbital, while in the octahedron BiO_6 with 20 electrons, the antibonding orbital is filled as shown in Fig. 1. It is quite natural that the $Bi\underline{L}^2O_6$ octahedra have stiff quasimolecular Bi–O bonds and a smaller radius, while the BiO_6 octahedra represent unstable molecules with the filled antibonding orbital and a larger radius.

Thus, in $BaBiO_3$ one has an alternating system of the two types of the octahedral complexes filled with local pairs: the hole pairs in $Bi\underline{L}^2O_6$ complexes and the electron pairs in BiO_6 complexes. In other words, the parent compound is a system with the real-space [33] or hard-core [16] bosons (i.e., with at most one boson per site).

The local pair formation in $BaBiO_3$ was advocated previously, e.g., in Refs. [15, 16, 18, 34–38]. The binding mechanism for the pairs is probably of an electronic nature [16, 35] in accordance with Varma's picture of the pairing due to the skipping of the valence «4+» by the

Bi ion [35]. However, one cannot fully exclude the lattice mediated pairing [18, 34, 37] in accordance with de Jongh's statement [36] that the preference to retain the close-shell structures overcomes the Coulomb repulsion related to the intrasite bipolaron formation.

The local electronic structure of $BaBiO_3$ combined with the real-space local crystal structure is presented in Fig. 2*a*. There are no free fermionic carriers in this system, and the conductivity is only due to the transfer of the carrier pairs [18, 28]. Experimentally, $BaBiO_3$ shows a semiconducting-type behavior with the energy gap $E_a = 0.24$ eV. This transport gap does not show up in photoconductivity, optical absorption, and photoacoustic measurements [39] and can be explained only as a two-particle transport with the activation energy $2E_a$ due to the delocalization of pairs. From our point of view, the transport gap value is defined by the combined effect of the intersite Coulomb repulsion and the local lattice deformation due to the static breathing distortion.

The optical gap, in similarity with Varma's [35] suggestion, costs the energy

$$E_g = E_b + 2E_a = 2E(\mathrm{Bi\underline{L}^1O_6}) - \\ - [E(\mathrm{BiO_6}) + E(\mathrm{Bi\underline{L}^2O_6})] \quad (1)$$

and is observed experimentally as the optical conductivity peak at the photon energy $h\nu = 1.9$ eV [18]. (Here, E_b is the pair binding energy related to the dissociation of pairs.)

In accordance with Eq. (1), the optical excitation must produce a local lattice deformation via the transformation of the two different octahedra into equivalent ones: $\mathrm{Bi\underline{L}^2O_6}+\mathrm{BiO_6} \xrightarrow{h\nu} 2\mathrm{Bi\underline{L}^1O_6}$. Consequently, this dynamical local lattice deformation is manifested in the Raman spectra as an abnormally large amplitude of breathing-type vibrations of the oxygen octahedra if the resonance laser excitation with $h\nu = E_g$ is used [31, 37, 40]. The abrupt decrease of the mode amplitude was observed when lasers with different wavelengths were used [40].

It is important to emphasize that there are no free fermions in the system. Only the excited fermions can be produced by the unpairing, and they do not give any contribution to the charge transport because of a high value of E_b. The bosonic and the fermionic subsystems are therefore separated both spatially and energetically, and hence, the Fermi–Bose mixture is absent in the parent compound.

This situation is illustrated in Fig. 3*a*, where we schematically present the one-particle density of states. For $x = 0$, the filled bosonic band is separated from the empty fermionic band (the excited band F') by the large optical gap E_g and from the empty bosonic band B by the smaller transport gap $2E_a$. The bosonic band plays the role of a conduction band for bosonic quasiparticles involved in the activation transport. In accordance with Ref. [41], the filled and empty bosonic bands have, respectively, the hole-like and electron-like dispersions in the representation of the one-particle density of states. Because bosons and fermions are always spatially separated (i.e., belong to different octahedra complexes), we show their densities of states in the different sides of the pictures.

C. Formation of the Fermi–Bose mixture

The substitution of the two K^+ ions for two Ba^{2+} ones modifies the BiO_6 complex to the $\mathrm{Bi\underline{L}^2O_6}$ one. As a result, the number of small stiff $\mathrm{Bi\underline{L}^2O_6}$ octahedra increases as $n_0(1+x)/2$ and the number of large soft BiO_6 octahedra decreases as $n_0(1-x)/2$, where $n_0 = 1/a^3$ is the number of unit cells and a is the lattice parameter. Clusters of the $\mathrm{Bi\underline{L}^2O_6}$ complexes are formed with doping, which contracts the lattice because of small radii and the rigid bonds of the $\mathrm{Bi\underline{L}^2O_6}$ complexes.

The changes in the crystal structure are accompanied by essential changes in the local electronic structure. A spatial overlap of the $\underline{\mathrm{L}}^2$ levels leads to their splitting into an empty fermionic-like band F inside the $\mathrm{Bi\underline{L}^2O_6} - \ldots - \mathrm{Bi\underline{L}^2O_6}$ Fermi cluster (see Fig. 2*b*). In the doping range $x < 0.37$, this sufficiently narrow band is still separated from the occupied Bi6*s*–O2*p* subband. The number of the empty electronic states in the F band increases with x as $\hat{n}_F = n_0(1+x)$, while the number of the local electron pairs decreases as $n_B = n_0(1-x)/2$.

The free motion of the pairs is still prevented by the intersite Coulomb repulsion ($E_a \neq 0$), which is screened inside the clusters, however. When the Fermi clusters are formed, the conductivity occurs because of the motion of the pairs through the clusters of different lengths. The BKBO compounds demonstrate a semiconducting-type conductivity changing from a simple activation type to the Mott's law with variable-range hopping [42].

At the doping level $x \approx 0.37$ (see Fig. 2*c* and Fig. 3*c*), the following cardinal changes occur.

(i) The breathing and the rotational static lattice distortions transform to the dynamic ones. At the Bose and the Fermi cluster borders, where all the oxygen ions belong to both the BiO_6 and $\mathrm{Bi\underline{L}^2O_6}$ octahedra, the local breathing dynamic distortion is observed as the oxygen ion vibration in a double-well potential [21, 22].

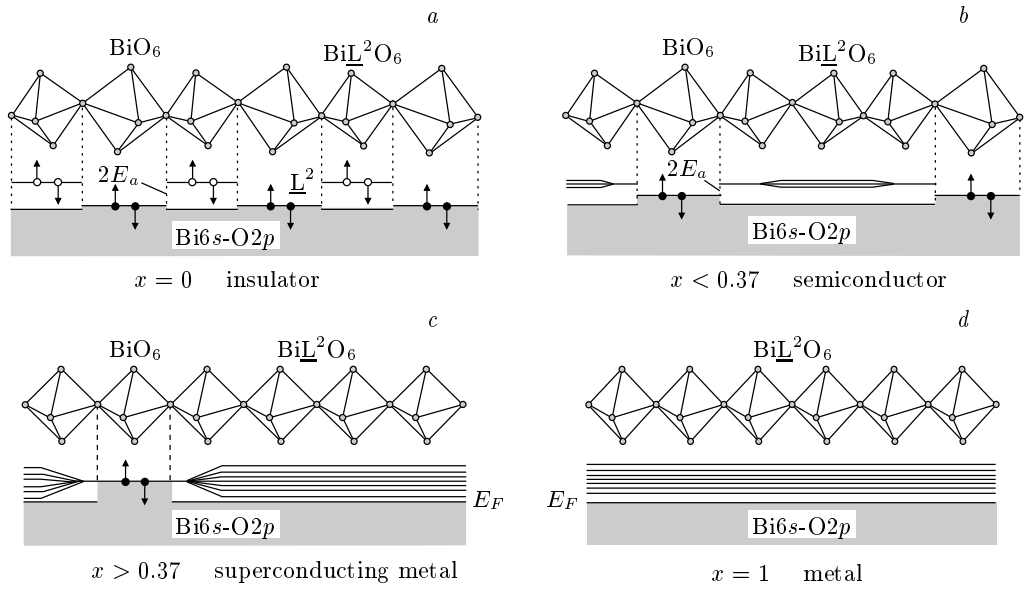

Fig. 2. The scheme of the insulator–metal phase transition for the K-doping of $Ba_{1-x}K_xBiO_3$ in the framework of the relationship between the local crystal and the local electronic structures. The local crystal structure of the octahedral complexes (at the top) and the local electronic structure (at the bottom) are shown in pictures (a)–(d). The occupied states of the $Bi6s$–$O2p$ valence band are marked by grey. $2E_a$ is the activation gap. Black and white circles with arrows denote, respectively, the electrons and the holes with the opposite spin orientations. (a) The monoclinic phase of the insulator $BaBiO_3$ compound. (b) The orthorhombic phase of a semiconducting BKBO at $0 < x < 0.37$. The splitting of the free level $\underline{L}^2$ at the spatial overlap of the $Bi\underline{L}^2O_6$ octahedra is sketched. (c) The undistorted cubic phase of a superconducting metal at $x > 0.37$. The formation of a Fermi-liquid state is shown arising due to the overlap of the unoccupied fermionic band F with the occupied $Bi6s$–$O2p$ valence band as the percolation threshold is reached. (d) The undistorted cubic phase of a nonsuperconducting metal at $x = 1$. A Fermi liquid state with the Fermi level E_F is shown

(ii) The infinite three-dimensional percolating Fermi cluster is formed from the $Bi\underline{L}^2O_6$ octahedra along the [100]-type directions. The empty fermionic band overlaps the filled one, and F therefore becomes a conduction band. Overcoming the percolation threshold provides the insulator–metal phase transition and the formation of the Fermi-liquid state for $x \geq 0.37$. The valence electrons previosly localized in the $Bi\underline{L}^2O_6$ complexes become itinerant inside the infinite Fermi cluster.

(iii) The pair localization energy disappears, $E_a \approx 0$, and therefore, local electron pairs originating from the BiO_6 complexes can move freely providing a bosonic contribution to the conductivity. In the metallic phase, two types of carriers are present: the itinerant electrons from the $Bi\underline{L}^2O_6$ complexes (fermions) and the delocalized electron pairs from the BiO_6 complexes (bosons). Although the normal state conductivity is mainly due to the fermionic subsystem, the contribution of the bosonic subsystem was also observed by Hellman and Hartford [43] as the two-particle normal state tunneling.

As a result, at doping levels $x \geq 0.37$, we have a new type of a spatially separated mixture of the bosonic and fermionic subsystems describing both metallic and superconducting properties of BKBO. We stress that because fermions and bosons belong to the complexes with different electronic structures, the Fermi and Bose subsystems are spatially separated at any doping level. These subsystems are related by

$$2n_B + \hat{n}_F = 2n_0, \tag{2}$$

and

$$\frac{2n_B}{\hat{n}_F} = \frac{1-x}{1+x}. \tag{3}$$

The pair destruction is prevented by a sufficiently high value of the binding energy, which becomes apparent as the pseudo-gap $E_b = E_g \approx 0.5$ eV [44] in superconducting compositions. The unpairing is possible only under the optical excitation to the band F' (see Fig. 3c), which does not play any role in the charge transport.

At $x = 1$, all the BiO_6 octahedra are transformed into the $Bi\underline{L}^2O_6$ ones. The Bose system disappears

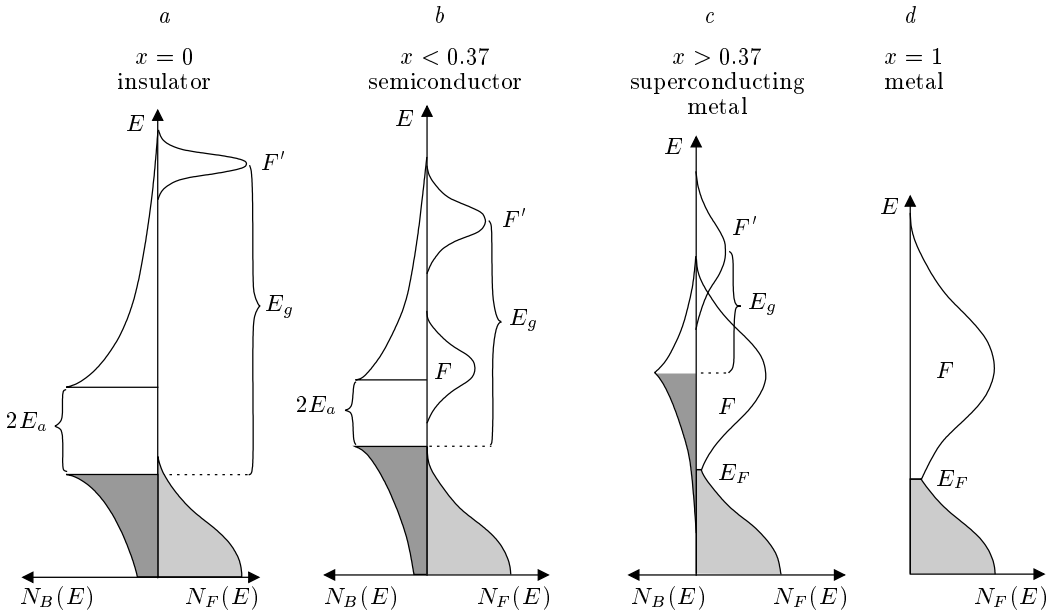

Fig. 3. A sketch of the one-particle density of states for $Ba_{1-x}K_xBiO_3$. The contributions of the bosons $N_B(E)$ and the fermions $N_F(E)$ are depicted separately because bosonic and fermionic states are spatially separated. The filled (dark grey) and the unoccupied (transparent) bosonic bands correspond, respectively, to the contributions of the electron and the hole pairs. The bands are separated by the activation gap $2E_a$, which is lowered with the doping level x. An empty fermionic band F' corresponding to the destruction of pairs is separated from the occupied bosonic band by the optical gap E_g. An empty fermionic band F is formed due to the splitting of the free level $\underline{L}^2$, which arises from the spatial overlap of the $Bi\underline{L}^2O_6$ octahedra. The filled fermionic band (grey) represents the $Bi6s$–$O2p$ valence band. The band F' and bosonic bands decrease as the doping increases, because the number of the electron pairs decreases, while the band F grows due to the increase of the number of free levels. A Fermi liquid state is formed (c), (d) as a result of the overlap between the F band and the $Bi6s$–$O2p$ valence band

($n_B = 0$) together with the excited fermionic band F'. Therefore, $KBiO_3$ must be a nonsuperconducting Fermi-liquid metal (see Fig. 2*d* and Fig. 3*d*).

We note that a metallic $KBiO_3$ compound exists only hypothetically because the potassium solubility limit $x \approx 0.5$ is exceeded in BKBO. However, $BaPbO_3$, which can be viewed as an electronic analogue of $KBiO_3$, demonstrates the metallic but not the superconducting properties. Recent attempts to synthesize $KBiO_3$ at a high pressure have shown that only $K_{1-y}Bi_yBiO_3$ with a partial replacement of the K^+ ions by the Bi^{3+} ones is formed [45]. This replacement must lead to the appearance of the BiO_6 octahedra with the local electron pairs, and the compound $K_{1-y}Bi_yBiO_3$ must therefore be superconducting in accordance with the above discussion. Indeed, superconductivity with $T_c = 10.2$ K was experimentally observed in this compound [45].

Our analysis implies that $BaPbO_3$ must be superconducting at a partial substitution of the Ba^{2+} ions for the trivalent ions because this substitution produces local electronic pairs as in the case of $K_{1-y}Bi_yBiO_3$. Thus, using the La^{3+} doping, it is possible to obtain the spatially separated Fermi–Bose mixture in $BaPbO_3$. Recently, we have successfully produced $Ba_{1-x}La_xPbO_3$ using the high-pressure synthesis technique. Superconductivity at $T_c = 11$ K observed in this new compound [46] is a direct evidence in favor of the above scenario.

At the end of this section, we note that our understanding of the insulating state in the parent $BaBiO_3$ is very similar to the theoretical model by Taraphder et al. [15, 16]. We agree with the authors of Refs. [15, 16] on the following principal positions: i) the presence of the electronic-mediated (Varma's type) pairing mechanism; ii) the existence of the charge $\pm 2e$ bosonic bound states that dominate transport properties of $BaBiO_3$; iii) the explanation of the nature of both the transport and the optical gaps.

However, our description of the K-doped systems strongly differs from their model. Going from insulating $BaBiO_3$ to superconducting BKBO ($x \geq 0.37$),

Taraphder et al. were forced to change the nature of the pairing mechanism from the real-space pairing to the k-space one. Thus their description of the superconducting state does not differ from the traditional BCS description that has been discussed for BKBO, e.g., in [12, 13, 47].

Using our EXAFS results [21, 22], we consistently explain the insulating and the superconducting states in BKBO within a single approach. In contrast to Refs. [15, 16], we showed that the real-space bosons do not disappear in the metalic region of BKBO and that they are responsible for superconductivity. At the same time, the Fermi liquid appears in the BKBO system because of the overlapping of the occupied valence band levels and the free ones when the percolation threshold $x = 0.37$ is overcome. An interplay of these Bose and Fermi subsystems explains the main properties of BKBO.

3. DISCUSSION

Taking the existence of the double-well potential in $Ba_{1-x}K_xBiO_3$ into account, one can consider superconductivity in this compound in the framework of the anharmonic models for HTSC [48, 49]. As shown in these models, if the oxygen ions move in a double-well potential, an order-of-magnitude enhancement of the electron–lattice coupling constant follows automatically from a consistent treatment of this motion.

However, as shown above, the double-well potential arises in the bismuthates from different electronic fillings of the nearest octahedra and the tunneling of local pairs between them. The existence of the double-well potential in the metallic phase of BKBO ($x \geq 0.37$) therefore indicates that the real-space bosons do not decay with doping. There are at least two additional experimental confirmations of this fact: i) the observation of the optical pseudogap in superconducting composition [44]; ii) the existence of two types of charge carriers with heavy and light masses [43, 50]. These experimental facts allow us to consider superconductivity in the bismuthates as the motion of local electronic pairs. This motion is correlated with the oxygen ion vibrations in the double-well potential and leads to the transformation of the Bose octahedral complexes to the Fermi ones and vice versa in the dynamical exchange process $BiO_6 \leftrightarrow Bi\underline{L}^2O_6$. The interplay between the Bose and the Fermi subsystems is closely related to the superconductivity analyzed below in more detail.

A. The Fermi–Bose mixture Hamiltonian

We first consider the Hamiltonian of the Fermi–Bose mixture (see, e.g., Ref. [51])

$$H = H_B + H_F + H_{FB} \tag{4}$$

in the spatially separated case,

$$\begin{aligned}
H_B &= \int d^3r\, \Phi^*(\mathbf{r}) \left[-\frac{\hbar^2}{2m_B}\nabla^2\right] \Phi(\mathbf{r}) + \\
&+ \frac{1}{2}U_{BB} \int d^3r\, d^3r' \Phi^*(\mathbf{r})\Phi^*(\mathbf{r}') \times \\
&\times \delta(\mathbf{r}-\mathbf{r}')\Phi(\mathbf{r}')\Phi(\mathbf{r}), \\
H_F &= \int d^3R\, \Psi^*_\alpha(\mathbf{R}) \left[-\frac{\hbar^2}{2m_F}\nabla^2\right] \Psi_\alpha(\mathbf{R}) + \\
&+ \frac{1}{2}U_{FF} \int d^3R\, d^3R' \Psi^*_\alpha(\mathbf{R})\Psi^*_\beta(\mathbf{R}') \times \\
&\times \delta(\mathbf{R}-\mathbf{R}')\Psi_\beta(\mathbf{R}')\Psi_\alpha(\mathbf{R}), \\
H_{FB} &= \int d^3R\, d^3r\, \Phi^*(\mathbf{r})\Psi^*_\alpha(\mathbf{R}) \times \\
&\times U_{FB}(\mathbf{r}-\mathbf{R})\Phi(\mathbf{r})\Psi_\alpha(\mathbf{R}),
\end{aligned} \tag{5}$$

where Φ and Ψ_α are bosonic and fermionic operators, and m_B and m_F are the effective masses of bosons and fermions. The most important property of Eq. (5) is that fermions and bosons are spatially separated, and moreover, the potential U_{FB} has a double-well shape at the boundary between the bosonic and fermionic subsystems. This fact is crucial for matching our model with experimental data on the local structure and for the explanation of superconductivity. Obviously, realistic Hamiltonians are more complicated, and the quantities U_{BB}, U_{FF}, and U_{FB} include not only the direct interactions between bosons and fermions, but also indirect interactions via the lattice. The last contribution could be dynamical in principle, and the picture could therefore change in time, thereby leading to a dynamical version of the real-space separation. We note that the bosonic Hamiltonian H_B in Eq. (4) is generated from the electronic band with a strong attraction between electrons (see Refs. [15, 16, 41]). We thus have two generic spatially separated electronic bands: one with a strong attraction between electrons and the other with a repulsion.

We must solve Hamiltonian (4) together with the equation for the particle number conservation obtained from Eqs. (2),

$$2n = \frac{2N}{\Omega} = \frac{1}{\Omega}\int 2n_B(\mathbf{r})\, d^3r + \frac{1}{\Omega}\int \hat{n}_F(\mathbf{R}) d^3R, \tag{6}$$

where

$$n_B(\mathbf{r}) = \langle \Phi^*(\mathbf{r})\Phi(\mathbf{r})\rangle,$$
$$\hat{n}_F(\mathbf{R}) = \sum_\alpha \langle \Psi^*_\alpha(\mathbf{R})\Psi_\alpha(\mathbf{R})\rangle, \qquad (7)$$

and Ω is the volume of the system. In accordance with Eqs. (3), we also have $2n_B/\hat{n}_F = (1-x)/(1+x)$.

We consider the system of equations (4)–(7) in the Hartree–Fock approximation. By analogy with the Fermi–Bose mixture ^{7}Li–^{6}Li in a magnetic trap [51], it is convenient to introduce the effective external potentials for fermions $U_{ext}(\mathbf{R})$ and bosons $U_{ext}(\mathbf{r})$ as

$$U_{ext}(\mathbf{r}) = \frac{1}{\Omega}\int U_{FB}(\mathbf{r}-\mathbf{R})\hat{n}_F(\mathbf{R})\, d^3R, \qquad (8)$$

$$U_{ext}(\mathbf{R}) = \frac{1}{\Omega}\int U_{FB}(\mathbf{r}-\mathbf{R})n_B(\mathbf{r})d^3r. \qquad (9)$$

Following Ref. [52], we then obtain

$$H_{HF} = \tilde{H}_B + \tilde{H}_F,$$

$$\tilde{H}_B = \int d^3r\, \Phi^*(\mathbf{r})\left[-\frac{\hbar^2}{2m_B}\frac{\partial^2}{\partial \mathbf{r}^2} + U_{BB}(\mathbf{r})n_B(\mathbf{r}) + U_{ext}(\mathbf{r})\right]\Phi(\mathbf{r}), \qquad (10)$$

$$\tilde{H}_F = \int d^3R\, \Psi^*_\alpha(\mathbf{R})\left[-\frac{\hbar^2}{2m_F}\frac{\partial^2}{\partial \mathbf{R}^2} + U_{FF}(\mathbf{R})\hat{n}_F(\mathbf{R}) + U_{ext}(\mathbf{R})\right]\Psi_\alpha(\mathbf{R}). \qquad (11)$$

Equations (10) and (11) self-consistently describe the interaction between the Fermi and Bose subsystems. However, in contrast to the Fermi–Bose mixture models discussed previously (see Sec. 1), the relation between the concentration of the bosonic and fermionic quasiparticles is independent of the temperature and depends only on the doping level x in accordance with Eq. (3).

The theoretical analysis of the above equations is beyond the scope of this paper and will be published elsewhere. We only note that the potential $U_{ext}(\mathbf{r})$ in (10), which is the contraction of the Fermi–Bose interaction potential $U_{FB}(\mathbf{r}-\mathbf{R})$ with the fermionic density $\hat{n}_F(\mathbf{R})$, also has a double-well shape, and the real-space bosons therefore live in the effective double-well external potential. The maximum of this external potential corresponds to the point $\mathbf{r} = \mathbf{R}$ at the boundary between the Fermi and the Bose clusters. Our estimate for the superconductivity critical temperature is heavily based on this fact.

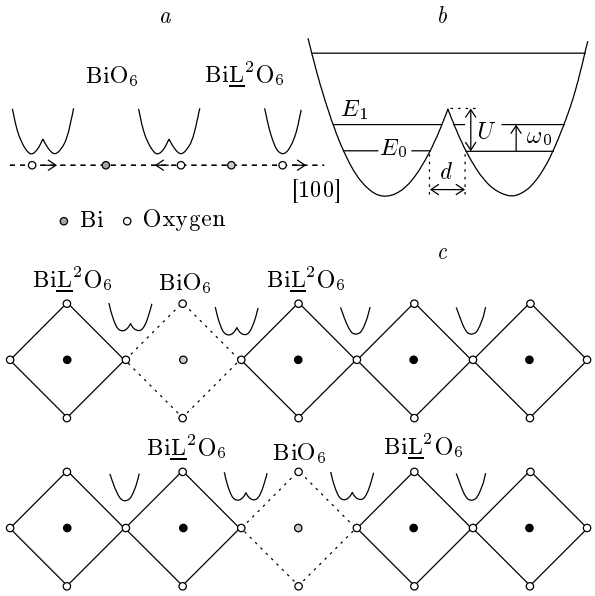

Fig. 4. A sketch of the dynamic exchange $BiO_6 \leftrightarrow Bi\underline{L}^2O_6$ is shown in the BiO_2 plane of the octahedra. (a) The breathing mode of the vibrations along the [100]-type direction of two neighboring octahedra with different electronic structures. The BiO_6 octahedron transforms to the $Bi\underline{L}^2O_6$ one and vice versa due to the electron pair tunneling between the octahedra. An oxygen ion belonging to these octahedra oscillates in the double-well potential. An oxygen ion belonging to the equivalent neighboring $Bi\underline{L}^2O_6$ octahedra oscillates in a simple parabolic potential. (b) The double-well potential with the energy levels for the vibration of the oxygen ion. The following parameters describe the tunneling barrier between the wells in $Ba_{0.6}K_{0.4}BiO_3$ at low temperatures [22]: the tunneling frequency $\omega_0 \approx 200$ K, the barrier height $U \approx 500$ K, the barrier width $d \approx 0.07$ Å. (c) The motion of a local electron pair centered on the BiO_6 octahedron through the $Bi\underline{L}^2O_6$ ... $Bi\underline{L}^2O_6$ Fermi cluster. For detailed explanations, see the text

B. Superconductivity in $Ba_{1-x}K_xBiO_3$

Taking the existence of the double-well potential in $Ba_{1-x}K_xBiO_3$ into account, one can consider superconductivity in this compound as a long-range order that is established via the local pair tunneling from one Bose cluster to a nearest one over the Fermi cluster along [100]-type directions.

The pair transfer process correlated with the oxygen vibration (in other words, the dynamic exchange) is illustrated in Fig. 4. The oxygen belonging to the two neighboring octahedra BiO_6 and $Bi\underline{L}^2O_6$ vibrates in the double-well potential, and hence, the electron

pair tunneling between the neighboring octahedra occurs when the ion tunnels through the potential barrier between the wells. Because of this interconnection between the pair and the oxygen tunneling processes, we can estimate the matrix element of the pair tunneling as $t_B \propto \omega_0 e^{-D}$, where ω_0 is the tunneling frequency,

$$D = \frac{1}{\hbar}\int\limits_{x_0}^{x_1} |p|dx \approx \frac{d}{\hbar}\sqrt{2MU}$$

is the semiclassical transparency of the barrier in the double-well potential, U and d are the barrier height and width, and M is the oxygen ion mass. We note that the relatively small tunneling frequency $\omega_0 = 200\,\mathrm{K}$ (see Fig. 4) already incorporates all the polaronic effects.

A local pair is transferred from one Bose cluster to the nearest one over a Fermi cluster, which, depending on the doping level, consists of several octahedra. The pairs overcome the Fermi cluster step by step. A single step corresponding to the pair transfer into a neighboring octahedron occurs simultaneously with the oxygen ion tunneling in the double-well potential. The tunneling frequency ω_0 is therefore the same for each step. Assuming that the steps are independent events, the probability of overcoming the Fermi cluster can be obtained as the product of the probabilities of each step. The matrix element of the pair tunneling through the Fermi cluster can then be estimated as $\hat{t}_B \propto \omega_0 e^{-\langle N\rangle D}$, where the average number of steps (which is proportional to the Fermi cluster linear size) can be obtained from the ratio of the concentrations of the $\mathrm{Bi\underline{L}^2O_6}$ and BiO_6 octahedra. This gives the number of steps

$$\langle N\rangle \approx \left(\frac{1+x}{1-x}\right)^{1/3}.$$

A natural assumption is that the critical temperature of the onset of superconductivity is of the order of the Bose–Einstein condensation temperature $T_c \propto \hat{t}_B a^2 n_B^{2/3}$ in the bosonic system with the large effective mass $m_B \propto 1/\hat{t}_B a^2$. We recall that $a^3 n_B = (1-x)/2$ in our case. For the parameters of the double-well potential obtained in Ref. [22] (see also Fig. 4), we estimated $T_c \sim 50\,\mathrm{K}$ in $Ba_{0.6}K_{0.4}BiO_3$, which is larger than the measured $T_c \approx 30$ K.

However, this estimate does not account for the phase coherence arising due to the relation between the vibrations of oxygen ions and the transfer of pairs. When a pair is transferred from one octahedron to another, the lattice has sufficient time to relax due to the longitudinal stretching phonons, each time forming a new configuration before the next tunneling event occurs. Taking the breathinglike character of the oxygen ion vibrations in the double-well potential into account (see Fig. 4), it is natural to suppose that the breathing mode of each octahedron is coordinated with its neighbors to guarantee a resonant tunneling along [100]-type axes in the system.

From the dispersion of longitudinal phonon modes studied by the inelastic neutron scattering [53], it follows that the breathing-type vibrations with the wave vector $q_b = (\pi/a, 0, 0)$ are energetically favorable in the superconducting compositions of BKBO. Hence, a long-range correlation of vibrations must occur at low temperatures when only the low-energy states are occupied. The bandwidth of the longitudinal stretching mode is of the order 100 K, and the temperature $T \sim T_c$ is sufficiently high to excite the non-breathing-type longitudinal stretching phonons with the wave vectors shorter than q_b. The thermal excitation of these phonons leads to the destruction of the long-range correlation between the breathing-type vibrations, and hence destructively affects the long-range phase coherency of the local pair transfer.

We note that the anomalous dispersion of the longitudinal stretching phonons observed in Ref. [53] reflects the lattice softening with the decrease of temperature due to the existence of a double-well potential in the superconducting compositions of BKBO. A similar dispersion was also observed in the high-T_c cuprates $La_{1.85}Sr_{0.15}CuO_4$ and $YBa_2Cu_3O_7$ [54]. The problem of the T_c limitation due to the phase coherence destruction is now extensively discussed (see [55] for a review). In view of the recent experimental evidence by Müller et al. [56] for the coexistence of small bosonic and fermionic charge carriers in $La_{2-x}Sr_xCuO_4$, we also envisage applying our scenario to HTSC cuprates. Because the underdoped HTSC-materials are similar to the phase separation on antiferromagnetic (AFM) and paramagnetic (PM) clusters [57–59], we suppose that the lattice can here play an assistant role by providing a pair tunneling between the superconducting PM metallic clusters via the insulating AFM barrier. It can also serve as a limitation for the estimate of the effective critical temperature for the superconducting transition in cuprates.

4. CONCLUSIONS

We briefly summarize the key positions of our concept.

1. The parent compound $BaBiO_3$ represents a sys-

tem with the initially preformed local electron and hole pairs. Each pair is spatially and energetically localized inside the octahedron volume. The localization energy of a pair determines the transport activation gap E_a. The binding energy of a pair is given by $E_b = E_g - 2E_a$, where E_g is the optical gap.

2. The spatially separated Fermi–Bose mixture of a new type is possibly realized in the superconducting compositions $Ba_{1-x}K_xBiO_3$ for $x \geq 0.37$. The bosonic bands are responsible for the two-particle normal state conductivity. The overlap of the empty fermionic band F with the occupied valence band Bi6s–O2p provides the insulator–metal phase transition and produces the Fermi-liquid state. This state strongly shunts the normal state conductivity arising from the two-particle Bose transport.

3. The fermionic band F' connected with the pair destruction does not play any role in the transport. The excitation energy is sufficiently high to guarantee against the destruction of bosons (the pair binding energy for superconducting compositions is $E_b \approx 0.5$ eV).

4. The pair localization energy is absent for $x \geq 0.37$ ($E_a = 0$), and therefore, the bosonic and the fermionic subsystems are separated only spatially. The interplay between them is due to the dynamic exchange $Bi\underline{L}^2O_6 \leftrightarrow BiO_6$, which causes the free motion of local pairs in the real space.

5. The pairing mechanism in the bismuthates is more likely of the Varma's type (because of skipping the «4+» valence by the Bi ion) rather than of the phonon-mediated origin. The existence of local pairs and their tunneling between the neighboring octahedra are closely related to the presence of a double-well potential that describes the vibration of the oxygen ions. The lattice is more likely involved in the superconductivity by providing the phase coherence for the motion of local pairs in the real space.

We finally emphasize that the scenario of the Fermi–Bose mixture allows us to qualitatively describe the insulator–metal phase transition and the superconducting state in BKBO in the framework of a single approach. To some extent, this scenario explains the contradictions between the result of the local sensitive and integral experimental methods [18–24, 31, 40, 53]. In addition, we successfully synthesized new superconducting oxide $Ba_{1-x}La_xPbO_3$ that can be considered as a direct evidence in favor of our model.

Nevertheless, additional experiments are required to make a definite conclusion about the nature of superconductivity in these systems.

We propose two direct experiments to test our model. (i) To provide the Raman scattering experiment of the superconducting $Ba_{0.6}K_{0.4}BiO_3$ compound using a resonance optical excitation in the range of the optical pseudogap $E_g \approx 0.5$ eV. In this case, a sharp increase of the amplitudes of some Raman modes due to local dynamic distortions must be observed at the pair destruction energy in accordance with our model. (ii) To provide measurements of the inelastic neutron scattering in the $Ba_{0.5}K_{0.5}BiO_3$ and $BaPbO_3$ samples. We expect that the dispersion of the longitudinal stretching mode should decrease with changing the K doping from $x = 0.4$ to $x = 0.5$ and should be absent in the metallic $BaPbO_3$ compound.

Moreover, it is important to carry out more precise measurements of the specific heat in the bismuthates for $T \sim T_c$. In the three-dimensional Bose gas, the specific heat behaves as $C_B \sim (T/T_c)^{3/2}$ for the temperatures $T < T_c$ and $C_B = \text{const}$ for $T \gg T_c$. As a result, there is a λ-point behavior of the specific heat for $T \sim T_c$. However, the Fermi–Bose mixture gives an additional contribution from the Fermi gas, $C_F \sim \gamma T$. This contribution could in principle destroy the λ-point behavior of the specific heat in the Fermi–Bose mixture. We note that the currently available experimental results in the bismuthates [60] signal a smooth behavior of the specific heat near T_c, because in all the experiments, the contributions of the Fermi and Bose gases are masked by a larger lattice contribution.

We acknowledge fruitful discussions with N. M. Plakida, Yu. Kagan, P. Fulde, P. Woelfe, and A. N. Mitin. This work was supported by the Russian Foundation for Basic Research (Grant № 99-02-17343) and Program «Superconductivity» (Grant № 99010). M. Yu. K. is grateful for the grant № 96-15-96942 of the President of Russia.

REFERENCES

1. M. R. Shafroth, Phys. Rev. B **100**, 463 (1955); M. R. Shafroth, Solid State Phys. **10**, 422 (1960).

2. A. S. Alexandrov and J. Ranninger, Phys. Rev. B **23**, 1796 (1981).

3. G. M. Eliashberg, Sov. Phys. JETP **16**, 780 (1963).

4. A. J. Leggett, in *Modern Trends in Theory of Condensed Matter. Lecture Notes of the 1979 Karpatz Winter School*, ed. by A. Pekalski and J. Przystowa, Springer-Verlag, Berlin (1980), p. 14.

5. P. Nozieres and S. Schmitt-Rink, J. of Low-Temp. Phys. **59**, 195 (1985).

6. J. Ranninger and S. Robaszkiewicz, Physica B **135**, 468 (1985).

7. B. K. Chakraverty, J. Ranninger, and D. Feinberg, Phys. Rev. Lett. **81**, 433 (1998).

8. P. W. Anderson, Science **235**, 1196 (1987).

9. V. B. Geshkenbein, L. B. Ioffe, and A. I. Larkin, Phys. Rev. B **55**, 3173 (1997).

10. Ch. Rener, B. Revaz, J.-Y. Genoud et al., Phys. Rev. Lett. **80**, 149 (1998).

11. L. F. Mattheiss and D. R. Hamann, Phys. Rev. B **28**, 4227 (1983).

12. M. Shirai, N. Suzuki, and K. Motizuki, J. Phys.: Condens. Matter **2**, 3553 (1990).

13. G. Vielsack and W. Weber, Phys. Rev. B **54**, 6614 (1996).

14. A. I. Liechtenstein, I. I. Mazin, C. O. Rodriguez et al., Phys. Rev. B **44**, 5388 (1991).

15. A. Taraphder, H. R. Krishamurthy, R. Pandit et al., Europhys. Lett. **21**, 79 (1993).

16. A. Taraphder, H. R. Krishamurthy, R. Pandit et al., Phys. Rev. B **52**, 1368 (1995).

17. V. Meregalli and S. Y. Savrasov, Phys. Rev. B **57**, 14453 (1998).

18. S. Uchida, K. Kitazawa, and S. Tanaka, Phase Transition **8**, 95 (1987).

19. M. Qvarford, V. G. Nazin, A. A. Zakharov et al., Phys. Rev. B **54**, 6700 (1996).

20. N. V. Anshukova, A. I. Golovashkin, V. S. Gorelik et al., J. Molecular Structure **219**, 147 (1990).

21. A. P. Menushenkov, K. V. Klementev, P. V. Konarev et al., Pis'ma Zh. Eksp. Theor. Fis. **67**, 977 (1998).

22. A. P. Menushenkov and K. V. Klementev, J. Phys.: Condens. Matter **12**, 3767 (2000).

23. S. Salem-Sugui, Jr., E. E. Alp, S. M. Mini et al., Phys. Rev. B **43**, 5511 (1991).

24. Y. Yacoby, S. M. Heald, and E. A. Stern, Solid State Commun. **101**, 801 (1997).

25. R. J. Cava, B. Batlogg, J. J. Krajewski et al., Nature **332**, 814 (1988).

26. Shiyou Pei, J. D. Jorgensen, B. Dabrowski et al., Phys. Rev. B **41**, 4126 (1990).

27. D. E. Cox and A. W. Sleight, Acta Crystallogr. B **35**, 1 (1989).

28. A. P. Menushenkov, Nucl. Instr. & Meth. in Phys. Res. A **405**, 365 (1998).

29. Shiyou Pei, J. D. Jorgensen, B. Dabrowski et al., Phys. Rev. B **41**, 4126 (1990).

30. A. W. Sleight, J. L. Gillson, and P. E. Bierstedt, Solid State Commun. **17**, 27 (1975).

31. Shunji Sugai, Jap. J. of Appl. Phys. **26** Suppl. 26-3, 1123 (1987).

32. Y. J. Uemura, B. J. Sternlieb, D. E. Cox et al., Nature **335**, 151 (1988).

33. N. Mott, Supercond. Sci. Technol. **4**, S59 (1991).

34. T. M. Rice and L. Sneddon, Phys. Rev. Lett. **47**, 689 (1981).

35. C. M. Varma, Phys. Rev. Lett. **61**, 2713 (1988).

36. L. J. De Jongh, Physica C **152**, 171 (1998).

37. S. Sugai, Solid State Commun. **72**, 1187 (1989).

38. J. Yu, X. Y . Chen, and W. P. Su, Phys. Rev. B **41**, 344 (1990).

39. S. Tajima, S. Uchida, A. Masaki et al., Phys. Rev. B **32**, 6302 (1985).

40. S. Tajima, M. Yoshida, N. Koshizuka et al., Phys. Rev. B **46**, 1232 (1992).

41. M. Yu. Kagan, R. Frésard, M. Capezzali, and H. Beck, Phys. Rev. B **57**, 5995 (1998).

42. E. S. Hellman, B. Miller, J. M. Rosamilia et al., Phys. Rev. B **44**, 9719 (1991).

43. E. S. Hellman and E. H. Hartford, Jr., Phys. Rev. B **52**, 6822 (1995).

44. S. H. Blanton, R. T. Collins, K. H. Kelleher et al., Phys. Rev. B **47**, 996 (1993).

45. N. R. Khasanova, A. Yamamoto, S. Tajima et al., Physica C **305**, 275 (1998).

46. A. P. Menushenkov, A. V. Tsvyashchenko, D. V. Eremenko et al., Fiz. Tverd. Tela **43**, 591 (2001).

47. Wei Jin, Macros H. Degani, Rajiv K. Kalia et al., Phys. Rev. B **45**, 5535 (1992).

48. N. M. Plakida, V. L. Aksenov, and S. L. Drechsler, Europhys. Lett. **4**, 1309 (1987).

49. J. R. Hardy and J. W. Flocken, Phys. Rev. Lett. **60**, 2191 (1988).

50. J. H. Lee, K. Char, Y. W. Park et al., Phys. Rev. B **61**, 14815 (2000).

51. T. Mijakawa, T. Suzuki, and H. Yabu, Phys. Rev. A **62**, 063613 (2000).

52. M. J. Bijlsma, B. A. Heringa H. T. C. Stoof, Phys. Rev. A **61**, 063613 (2000).

53. M. Braden, W. Reichardt, W. Schmidbauer et al., J. of Supercond. **8**, 595 (1995).

54. L. Pintschovius and W. Reichardt, in *Physical Properties of High Temperature Superconductors IV*, ed. by D. M. Ginsberg, World Scientific, Singapore–New Jersey–London–Hong Kong (1994).

55. J. Orenstein and A. J. Mills, Science **288**, 468 (2000).

56. K. A. Müller, Guo meng Zhao, K. Conder et al., J. Phys.: Condens. Matter **10**, L291 (1998).

57. D. Jorgensen, B. Dabrowski, S. Pei et al., Phys. Rev. B **38**, 11337 (1988).

58. V. Yu. Pomyakushin, A. A. Zakharov, A. M. Balagurov et al., Phys. Rev. B **58**, 12350 (1998).

59. V. J. Emery and S. A. Kivel'son, Physica C **209**, 597 (1993).

60. S. E. Stupp, M. E. Reeves, D. M. Ginsberg et al., Phys. Rev. B **40**, 10878 (1989).